

# Dynamic converse magnetoelectric effect in ferromagnetic nanostructures with electric-field-dependent interfacial anisotropy

G. Viaud<sup>1,2</sup> and N. A. Pertsev<sup>2,3,\*</sup><sup>1</sup>*École Centrale Paris, 92295 Châtenay-Malabry, France*<sup>2</sup>*A. F. Ioffe Physical-Technical Institute, 194021 St. Petersburg, Russia*<sup>3</sup>*St. Petersburg State Polytechnical University, 195251 St. Petersburg, Russia*

(Received 30 December 2013; revised manuscript received 30 July 2014; published 27 August 2014)

Magnetization oscillations excited by microwave voltages in ferromagnetic nanostructures having electric-field-dependent interfacial anisotropy are described theoretically. By calculating frequency dependencies of complex susceptibilities we show that this dynamic magnetoelectric effect acquires anomalous characteristics near thickness-induced spin reorientation transitions (SRTs) in nanolayers of cubic ferromagnets. Most importantly, the peak magnetoelectric susceptibilities may reach giant values exceeding  $10^{-6}$  s/m, and the tunability of the resonance frequency of the magnetization precession by a dc voltage increases drastically near the critical thickness or voltage inducing an SRT.

DOI: [10.1103/PhysRevB.90.064429](https://doi.org/10.1103/PhysRevB.90.064429)

PACS number(s): 75.85.+t, 75.30.Gw, 75.50.Bb, 75.75.-c

## I. INTRODUCTION

High-frequency magnetization oscillations in ferromagnets are usually excited by microwave magnetic fields [1] but this technique suffers from high power consumption and large spatial dispersion not suitable for nanoelectronic devices. Another approach is based on the use of spin-polarized currents created in conductive magnetic nanostructures, which exert a spin-transfer torque (STT) on the magnetization [2,3]. The STT effect renders it possible to induce coherent high-frequency magnetization dynamics in ferromagnetic films even by a dc current [4–6]. This phenomenon is employed in spin-torque nanoscale oscillators which create microwave output voltages owing to the magnetoresistance (see Ref. [7] and references therein). Importantly, the frequency of magnetization precession can be tuned over a range of several gigahertz by varying the current density [5], and output powers in the microwatt range compatible with applications for mobile telecommunications may be generated by magnetic tunnel junctions (MTJs) with MgO barriers [6]. Microwave currents flowing through MTJs have also been successfully employed to induce steady-state magnetization precession and to observe the STT-driven ferromagnetic resonance [8,9].

Although spin-polarized currents represent an efficient tool for the high-speed manipulation of magnetic nanostructures, the associated Ohmic losses are still too high for many applications. Hence there is an increasing interest in other methods that enable the control of magnetization dynamics by electric fields rather than by currents and can therefore greatly reduce the power consumption of spintronic devices. Recently, it was shown experimentally and theoretically that the surface/interface magnetic anisotropy of metallic ferromagnetic nanolayers is sensitive to the electric field created in an adjacent medium [10–15]. This remarkable feature opens the possibility to induce magnetization oscillations in ferromagnetic nanostructures directly by the applied voltage. Indeed, it has already been demonstrated that the ferromagnetic resonance can be excited by microwave-frequency

voltages applied to MgO-based MTJs with an ultrathin free layer [16,17]. The voltage-driven magnetization precession in MTJs can be employed for the development of microwave signal detectors with a high sensitivity [17,18].

In this paper, we describe theoretically the magnetization oscillations induced by an ac voltage applied to a nanostructure, where the magnetic anisotropy of a ferromagnetic nanolayer varies with the electric field created in the adjacent insulating one. This *dynamic converse magnetoelectric effect* is quantified by complex magnetoelectric susceptibilities calculated as functions of the excitation frequency. To demonstrate the role of the voltage-controlled anisotropy, we focus on nanostructures where the STT effect is absent or may be neglected (e.g., tunnel junctions comprising only one ferromagnetic electrode). Importantly, the theory takes into account the existence of thickness-induced spin reorientation transitions (SRTs) in cubic ferromagnets and predicts the appearance of magnetoelectric anomalies near these transitions.

## II. VOLTAGE-DRIVEN MAGNETIZATION OSCILLATIONS

We consider ferromagnet-insulator-metal trilayers, where the interfacial magnetic anisotropy depends on the electric field  $\mathbf{E}$  created in the insulating interlayer by a voltage source (Fig. 1). Our calculations are focused on ferromagnetic layers with a nanometric thickness and nanoscale in-plane dimensions. In such nanolayers, the interfacial anisotropy represents a significant part of the total magnetic energy, and a homogeneous spatial distribution may be assumed for the magnetization  $\mathbf{M}$ . Accordingly, we may describe the voltage-induced magnetization dynamics in the macrospin approximation using the Landau-Lifshitz-Gilbert (LLG) equation  $d\mathbf{M}/dt = -\gamma\mu_0\mathbf{M} \times \mathbf{H}_{\text{eff}} + (\alpha/M_s)\mathbf{M} \times d\mathbf{M}/dt$ , where  $\gamma$  is the gyromagnetic ratio,  $\mu_0$  is the permeability of the vacuum,  $\alpha$  is the dimensionless damping parameter,  $M_s$  is the saturation magnetization regarded as a constant quantity independent of the electric field  $\mathbf{E}$  [19], and  $\mathbf{H}_{\text{eff}}$  is the effective magnetic field defined by the relation  $\mathbf{H}_{\text{eff}} = -(1/\mu_0)\partial F/\partial\mathbf{M}$ , where  $F$  is the Helmholtz energy density of a ferromagnetic layer allowing for the presence of interfacial magnetic anisotropy  $F_{\text{IMA}}$  (see Appendix A).

\*Corresponding author: [pertsev.domain@mail.ioffe.ru](mailto:pertsev.domain@mail.ioffe.ru)

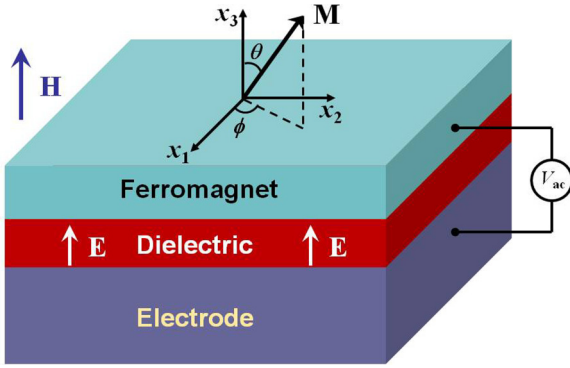


FIG. 1. (Color online) Schematic representation of a magnetic nanostructure having the form of a ferromagnet-dielectric-metal trilayer connected to a voltage source.

In our formulation, the energy density  $F_{\text{IMA}}$  has the form  $F_{\text{IMA}} = K_s m_3^2 / t_f$ , where  $K_s$  is the coefficient defining the total specific energy of two surfaces of a ferromagnetic layer having the thickness  $t_f$ , and  $m_3$  is the projection of the unit vector  $\mathbf{m} = \mathbf{M}/M_s$  on the  $x_3$  axis orthogonal to these surfaces. Since the first-principles calculations demonstrate a linear variation of  $K_s$  with the field intensity  $E_3$  [11], the dependence of this coefficient on the applied voltage  $V$  may be described by the relation  $K_s = K_{s0} + k_s V / t_b$ , where  $k_s = \partial K_s / \partial E_3$  is the sensitivity of  $K_s$  to the electric field  $\mathbf{E}$ , and  $t_b$  is the thickness of the insulating layer (barrier). Hence the effective magnetic field contains a voltage-dependent term of the form  $\Delta H_3^{\text{eff}}(V) = -2k_s(\mu_0 M_s t_f t_b)^{-1}(V_{\text{dc}} + V_{\text{ac}})m_3$ , where the applied voltage is taken to be the sum of dc and ac contributions. This relation immediately shows that weak ac voltages cannot induce magnetization oscillations when  $\mathbf{M}$  has an in-plane (IP) orientation ( $m_3 = 0$ ). Neither can the perpendicular-to-plane (PP) magnetic states ( $m_3 = \pm 1$ ) be destabilized because the voltage-dependent torque in the LLG equation vanishes ( $\mathbf{M} \times \Delta \mathbf{H}_{\text{eff}} = 0$ ). Therefore, we concentrate below on magnetic states with the vector  $\mathbf{M}$  inclined to the layer surfaces ( $0 < |m_3| < 1$ ), which usually requires the application of a suitably oriented magnetic field  $\mathbf{H}$ . It should be noted that, in nanolayers of cubic ferromagnets subjected to sufficiently strong voltages, magnetization oscillations may be induced even at the IP and PP static orientations of  $\mathbf{M}$ . This particular situation, which is discussed in Appendix B, occurs when the total applied voltage  $V = V_{\text{dc}} + V_{\text{ac}}$  periodically exceeds the critical voltage characterizing a voltage-driven SRT [11, 19].

The most convenient way to solve the LLG equation is to rewrite it in the spherical coordinates  $\theta$  and  $\phi$  defining the magnetization direction (see Fig. 1) [20]. Expressing the effective field  $\mathbf{H}_{\text{eff}}$  through the angular derivatives of the normalized free energy density  $f = F / (\mu_0 M_s^2)$  and introducing the dimensionless time  $\tau_\alpha = \gamma \mu_0 M_s t / (1 + \alpha^2)$ , we obtain the following system of differential equations:

$$\begin{aligned} \sin^2 \theta \frac{d\phi}{d\tau_\alpha} &= -\alpha \frac{\partial f}{\partial \phi} + \sin \theta \frac{\partial f}{\partial \theta}, \\ \sin \theta \frac{d\theta}{d\tau_\alpha} &= -\frac{\partial f}{\partial \theta} - \alpha \sin \theta \frac{\partial f}{\partial \theta}. \end{aligned} \quad (1)$$

For small deviations  $\delta\phi = \phi - \phi_0$  and  $\delta\theta = \theta - \theta_0$  from the initial equilibrium magnetization orientation defined by

the angles  $\phi_0$  and  $\theta_0$ , Eq. (1) can be linearized by replacing partial derivatives of  $f$  by appropriate terms in their Taylor expansions. Under the condition  $\theta_0 \neq \{0, \pi/2\}$ , the calculation of the linearized system of equations yields

$$\begin{aligned} \frac{d\delta\phi}{d\tau_\alpha} &= A_{11}\delta\phi + A_{12}\delta\theta + b_1(\tau_\alpha), \\ \frac{d\delta\theta}{d\tau_\alpha} &= A_{21}\delta\phi + A_{22}\delta\theta + b_2(\tau_\alpha), \end{aligned} \quad (2)$$

where

$$\begin{aligned} A_{11} &= \frac{1}{\sin \theta_0} \frac{\partial^2 f_{\text{st}}}{\partial \phi \partial \theta} - \frac{\alpha}{\sin^2 \theta_0} \frac{\partial^2 f_{\text{st}}}{\partial \phi^2}, \\ A_{12} &= \frac{1}{\sin \theta_0} \frac{\partial^2 f_{\text{st}}}{\partial \theta^2} - \frac{\alpha}{\sin^2 \theta_0} \frac{\partial^2 f_{\text{st}}}{\partial \phi \partial \theta}, \\ A_{21} &= -\frac{1}{\sin \theta_0} \frac{\partial^2 f_{\text{st}}}{\partial \phi^2} - \alpha \frac{\partial^2 f_{\text{st}}}{\partial \phi \partial \theta}, \\ A_{22} &= -\frac{1}{\sin \theta_0} \frac{\partial^2 f_{\text{st}}}{\partial \phi \partial \theta} - \alpha \frac{\partial^2 f_{\text{st}}}{\partial \theta^2}, \end{aligned} \quad (3)$$

$$b_1 = \frac{1}{\sin \theta_0} \frac{\partial f}{\partial \theta} - \frac{\alpha}{\sin^2 \theta_0} \frac{\partial f}{\partial \phi}, \quad b_2 = -\frac{1}{\sin \theta_0} \frac{\partial f}{\partial \phi} - \alpha \frac{\partial f}{\partial \theta}. \quad (4)$$

In Eqs. (3) and (4), all derivatives are taken at  $\phi = \phi_0$  and  $\theta = \theta_0$ , and  $f_{\text{st}}$  represents the energy density in the absence of excitation, which does not vary with time and has zero derivatives  $\partial f_{\text{st}} / \partial \phi$  and  $\partial f_{\text{st}} / \partial \theta$  in equilibrium. In our case of magnetization dynamics driven by voltage-dependent interfacial magnetic anisotropy, the quantities  $b_{1,2}$  are directly proportional to the applied ac voltage, namely,  $b_{1,2} = \tilde{b}_{1,2} V_{\text{ac}}$  with  $\tilde{b}_1 = -2k_s \cos \theta_0 / (\mu_0 M_s^2 t_f t_b)$  and  $\tilde{b}_2 = 2\alpha k_s \cos \theta_0 \sin \theta_0 / (\mu_0 M_s^2 t_f t_b)$ .

To find the steady-state solution of Eq. (2) describing the magnetization precession induced by an oscillating voltage  $V_{\text{ac}}$ , we employ the complex representation  $V_{\text{ac}} = \delta V_{\text{max}} \exp(i\omega t) = \delta V_{\text{max}} \exp(i\omega_\alpha \tau_\alpha)$  with a real amplitude  $\delta V_{\text{max}}$  for the voltage and seek for the solutions in the form  $\delta\phi = \delta\phi_{\text{amp}} \exp(i\omega_\alpha \tau_\alpha)$  and  $\delta\theta = \delta\theta_{\text{amp}} \exp(i\omega_\alpha \tau_\alpha)$ , where  $\omega_\alpha = \omega(1 + \alpha^2) / (\gamma \mu_0 M_s)$ . Then Eq. (2) reduces to a system of equations for the complex amplitudes  $\delta\phi_{\text{amp}}$  and  $\delta\theta_{\text{amp}}$ , which gives

$$\delta\phi_{\text{amp}} = \frac{-(A_{22} - i\omega_\alpha)\tilde{b}_1 + A_{12}\tilde{b}_2}{A_{11}A_{22} - A_{12}A_{21} - \omega_\alpha^2 - i\omega_\alpha(A_{11} + A_{22})} \delta V_{\text{max}}, \quad (5)$$

$$\delta\theta_{\text{amp}} = \frac{A_{21}\tilde{b}_1 - (A_{11} - i\omega_\alpha)\tilde{b}_2}{A_{11}A_{22} - A_{12}A_{21} - \omega_\alpha^2 - i\omega_\alpha(A_{11} + A_{22})} \delta V_{\text{max}}. \quad (6)$$

Using Eqs. (3)–(6) together with an appropriate relation for the free energy density  $f_{\text{st}}(\phi, \theta)$ , one can calculate the real and imaginary parts of  $\delta\phi_{\text{amp}}$  and  $\delta\theta_{\text{amp}}$  as a function of the frequency  $\nu = \omega/2\pi$  of the ac voltage applied to a ferromagnetic nanostructure.

In this work, we focused on nanostructures comprising (001)-oriented single-crystalline layers of cubic ferromagnets

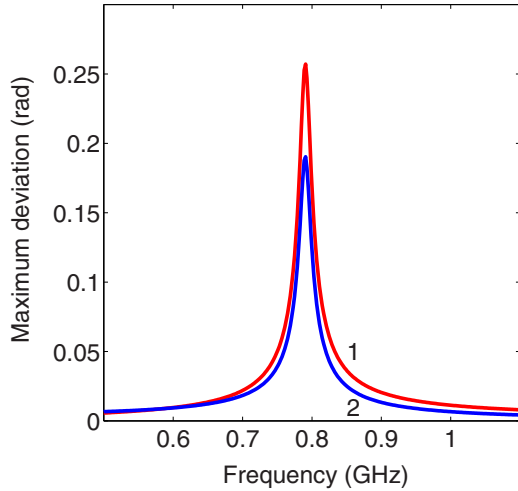


FIG. 2. (Color online) Magnitudes of the angular deviations  $\delta\phi$  (curve 1) and  $\delta\theta$  (curve 2) of the magnetization from the static orientation calculated as a function of frequency  $\nu$  of the applied ac voltage. The voltage amplitude  $\delta V_{\max}$  is taken to be 0.01 V, and the out-of-plane magnetic field  $H_3$  equals 100 Oe. The CoFeB layer has the thickness of 1.629 nm and almost in-plane magnetization orientation ( $\phi_0 = 0$ ,  $\theta_0 = 77^\circ$ ).

and employed an explicit expression for their energy density given in Ref. [21] (see Appendix A). The numerical calculations were performed for CoFeB alloys coupled to MgO using typical values of the involved material parameters:  $K_{s,0} = -1.3 \times 10^{-3} \text{ J m}^{-2}$  [22],  $k_s = -50 \mu\text{J m}^{-2} (\text{V nm}^{-1})^{-1}$  [23],  $M_s = 1.15 \times 10^6 \text{ A m}^{-1}$  [23], and  $\alpha = 0.01$  [22]. Using Eqs. (3)–(6) together with Eq. (A1), we calculated the frequency dependencies of the magnitudes of the magnetization's angular deviations  $\delta\phi$  and  $\delta\theta$  from the static orientation. The results obtained for the maximum angular deviations during the magnetization precession at  $\delta V_{\max} = 0.01 \text{ V}$  for a CoFeB layer coupled to MgO are presented in Fig. 2. It can be seen that these deviations show a peak at almost the same frequency but have different maximal values, which indicates an elliptical trajectory of the end of the magnetization vector  $\mathbf{M}$ .

### III. MAGNETOELECTRIC SUSCEPTIBILITIES AND THEIR EXPERIMENTAL DETERMINATION

Since the voltage-driven magnetization precession represents a dynamic converse magnetoelectric (ME) effect, the most important characteristics of this phenomenon are the complex ME susceptibilities  $\alpha_{i3} = \mu_0 \delta M_i / \delta E_3$  ( $i = 1, 2, 3$ ). Expressing the magnetization projections  $M_i$  on the coordinate axes  $x_i$  via the orientation angles  $\phi$  and  $\theta$ , we find

$$\alpha_{13} = \mu_0 M_s t_b \left( -\sin \theta_0 \sin \phi_0 \frac{\delta \phi_{\text{amp}}}{\delta V_{\max}} + \cos \theta_0 \cos \phi_0 \frac{\delta \theta_{\text{amp}}}{\delta V_{\max}} \right), \quad (7)$$

$$\alpha_{23} = \mu_0 M_s t_b \left( \sin \theta_0 \cos \phi_0 \frac{\delta \phi_{\text{amp}}}{\delta V_{\max}} + \cos \theta_0 \sin \phi_0 \frac{\delta \theta_{\text{amp}}}{\delta V_{\max}} \right), \quad (8)$$

$$\alpha_{33} = -\mu_0 M_s t_b \sin \theta_0 \frac{\delta \theta_{\text{amp}}}{\delta V_{\max}}. \quad (9)$$

Equations (7)–(9) were used to numerically calculate the real and imaginary parts of  $\alpha_{i3}$  for heterostructures comprising CoFeB-MgO bilayers. Representative frequency dependencies of these quantities, which correspond to a CoFeB layer with the static magnetization lying in the  $(x_1, x_3)$  plane ( $\phi_0 = 0$ ), are shown in Fig. 3. It can be seen that the imaginary part of the coefficients  $\alpha_{13}$  and  $\alpha_{33}$  displays a symmetric peak at the resonance frequency  $\nu_{\text{res}}$ , while the real part crosses zero at the frequency  $\nu_0 \cong \nu_{\text{res}}$  and has an antisymmetric dispersion with respect to  $\nu_0$ . In contrast,  $\alpha_{23}$  shows an opposite behavior [Fig. 3(b)], which can be explained by the similarity of this ME susceptibility to the off-diagonal components of the tensor of magnetic susceptibilities characterizing conventional ferromagnetic resonance. Furthermore, the analysis shows that the ME response curves of the two discussed types can be fitted by symmetric and antisymmetric Lorentzians with good accuracy. It should be noted that, since  $M_s = \sqrt{M_1^2 + M_2^2 + M_3^2}$  is regarded as a fixed quantity, ME coefficients satisfy the condition  $\sin \theta_0 (\cos \phi_0 \alpha_{13} + \sin \phi_0 \alpha_{23}) + \cos \theta_0 \alpha_{33} = 0$ , which reduces to  $\alpha_{13} = -\cot \theta_0 \alpha_{33}$  at  $\phi_0 = 0$ .

Remarkably, the peak values of ME susceptibilities strongly increase near the thickness-induced SRTs occurring in nanolayers of cubic ferromagnets. In epitaxial films of CoFeB alloys and other ferromagnetic materials with positive bulk magnetocrystalline anisotropy, this SRT in the absence of magnetic fields usually has the form of an abrupt transition between IP and PP magnetization orientations taking place at a critical thickness  $t_f^*$  [21]. For the discussed unstrained CoFeB layer coupled to MgO, the calculation gives  $t_f^*(V = 0) = 1.604 \text{ nm}$  (see Appendix A). Since  $K_{s,0} < 0$ , the PP orientation stabilizes at  $t_f \leq t_f^*$ , whereas the IP one becomes stable at  $t_f \geq t_f^*$ . In the presence of a magnetic field  $\mathbf{H}$  needed to create an inclined magnetization orientation, the critical thickness  $t_f^*$  changes (see Appendix A) and an abrupt (first-order) SRT may transform into a gradual (second-order) one [24].

Figures 4–6 show the real and imaginary parts of the ME coefficients  $\alpha_{13}$ ,  $\alpha_{23}$ , and  $\alpha_{33}$  plotted as functions of frequency of the driving ac voltage at different thicknesses  $t_f \geq t_f^*$  of the CoFeB layer. It can be seen that the ME peaks become higher and narrower as  $t_f$  approaches  $t_f^*(H_3)$  from above in the presence of a perpendicular-to-plane magnetic field  $H_3$ . A similar evolution is displayed by the ME coefficients when the CoFeB thickness increases up to  $t_f^*(H_1)$  at a nonzero in-plane magnetic field  $H_1$  needed to tilt the magnetization. The maximum values of  $\text{Re}[\alpha_{i3}]$  and  $\text{Im}[\alpha_{i3}]$  increase monotonically with decreasing difference  $|t_f - t_f^*|$  at both  $t_f \leq t_f^*(\mathbf{H})$  and  $t_f \geq t_f^*(\mathbf{H})$  when the magnetic field  $\mathbf{H}$  is inclined to the layer surfaces. In contrast, the ME susceptibilities become zero at  $t_f > t_f^*(H_1)$  and  $t_f < t_f^*(H_3)$  because under these conditions the CoFeB magnetization acquires IP ( $H_3 = 0$ ) and PP ( $H_1 = 0$ ) orientations, respectively.

The inspection of Figs. 4–6 also demonstrates that all characteristic frequencies decrease as the CoFeB layer thickness  $t_f$  approaches the critical value  $t_f^*$  corresponding to the size-driven SRT. The theoretical analysis shows that the thickness dependencies of these frequencies can be calculated analytically. However, the derived analytical relations are very cumbersome, except for the formula giving the frequency  $\nu_0$  at which  $\text{Re}[\alpha_{33}]$  goes to zero. This formula can be

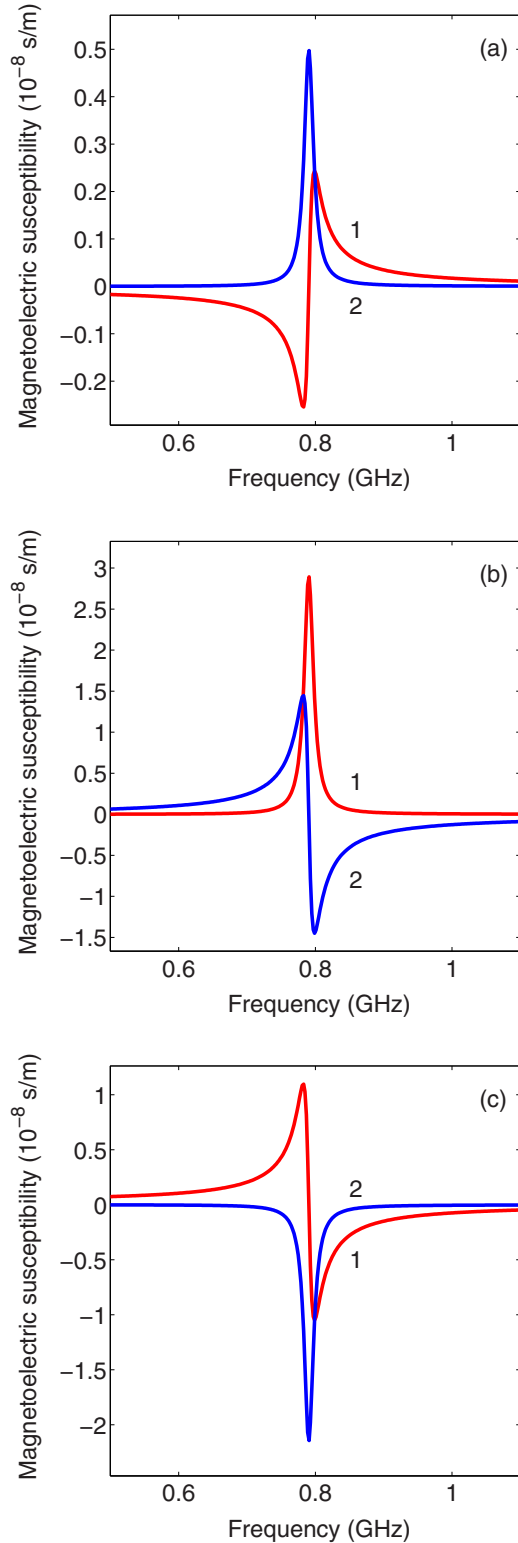


FIG. 3. (Color online) Frequency dependencies of the real (curve 1) and imaginary (curve 2) parts of the dynamic magnetoelectric coefficients  $\alpha_{13}$  (a),  $\alpha_{23}$  (b), and  $\alpha_{33}$  (c) calculated for the CoFeB-MgO nanostructure subjected to the out-of-plane magnetic field  $H_3 = 100$  Oe. The CoFeB layer has the thickness  $t_f = 1.629$  nm, negligible lattice strains, demagnetizing factors  $N_{11} = N_{22} = 0.008$ ,  $N_{33} = 0.984$ ,  $N_{12} = N_{13} = N_{23} = 0$ , and almost in-plane magnetization orientation ( $\phi_0 = 0$ ,  $\theta_0 = 77^\circ$ ). The MgO thickness is assumed to be 0.8 nm.

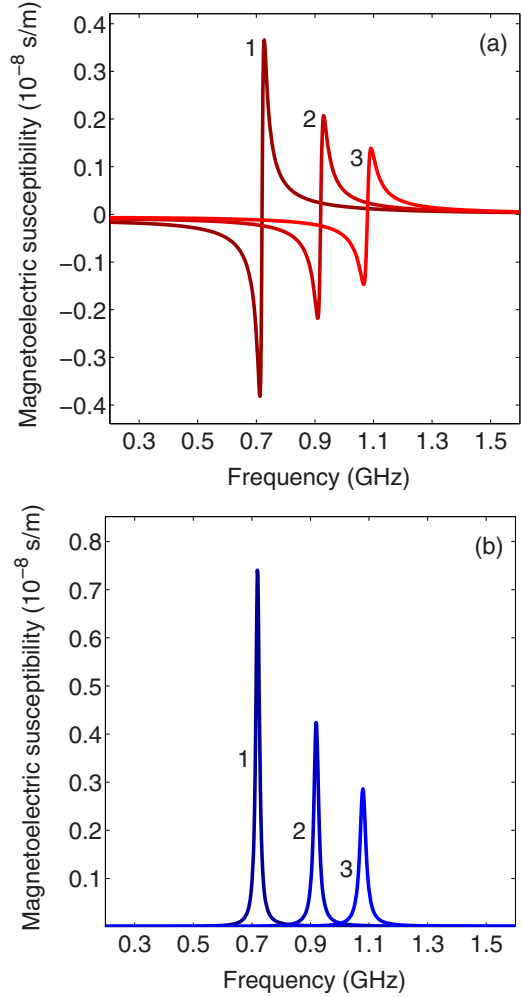


FIG. 4. (Color online) Evolution of the ME susceptibility  $\alpha_{13}$  with the CoFeB layer thickness near the size-induced SRT. The real (a) and imaginary (b) parts of  $\alpha_{13}$  are plotted as functions of the frequency  $\nu$  of the driving ac voltage. The thickness of the CoFeB layer subjected to the magnetic field  $H_3 = 100$  Oe increases from  $t_f^* = 1.624$  nm (curve 1) to  $t_f = 1.674$  nm (curve 3) with the step  $\delta t_f = 0.025$  nm.

written as

$$\nu_0 = \frac{\gamma \mu_0 M_s}{2\pi(1 + \alpha^2)} \sqrt{\frac{(A_{11}A_{22} - A_{12}A_{21})(A_{21} + \alpha \sin \theta_0 A_{11})}{(A_{21} - \alpha \sin \theta_0 A_{22})}}, \quad (10)$$

where  $A_{ij}$  are defined by Eq. (3). The numerical calculations indicate that Eq. (10) renders it possible to estimate with good accuracy the frequencies corresponding to the peaks of  $\text{Im}[\alpha_{33}]$  and  $\text{Re}[\alpha_{23}]$  as well.

Importantly, strong enhancement of maximum susceptibilities can also be achieved by applying a dc voltage  $V_{\text{dc}}$  to the MgO layer (see Fig. 7). This ME anomaly, with peak values exceeding  $10^{-6}$  s/m, appears when  $V_{\text{dc}}$  approaches the critical voltage  $V^*(t_f)$  inducing an SRT in a CoFeB layer with sufficiently small  $|t_f - t_f^*|$  [19]. In the presence of a dc voltage, the ME peaks also shift to higher or lower frequencies. Figure 8 shows the resonance frequency  $\nu_{\text{res}}$  maximizing the imaginary

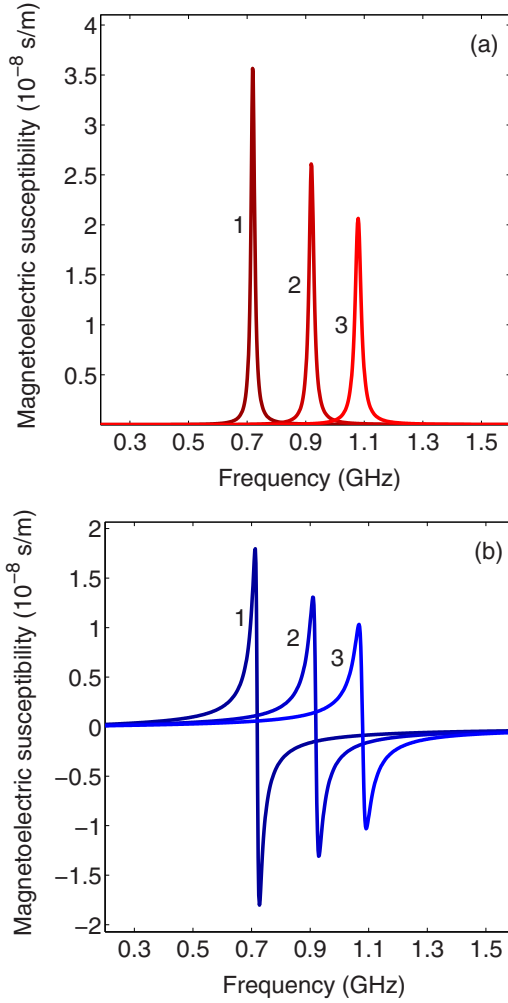


FIG. 5. (Color online) Evolution of the ME coefficient  $\alpha_{23}$  with the CoFeB layer thickness near the size-induced SRT. The real (a) and imaginary (b) parts of  $\alpha_{23}$  are plotted as functions of the frequency  $\nu$  of the driving ac voltage. The thickness of the CoFeB layer subjected to the magnetic field  $H_3 = 100$  Oe increases from  $t_f^* = 1.624$  nm (curve 1) to  $t_f = 1.674$  nm (curve 3) with the step  $\delta t_f = 0.025$  nm.

parts of the coefficients  $\alpha_{13}$  and  $\alpha_{33}$  plotted as a function of  $V_{dc}$ . It can be seen that  $\nu_{res}$  varies with voltage nonlinearly and strongly decreases near the critical value  $V^*(t_f)$ . Hence it is possible to achieve an efficient electrical tuning of the resonance frequency, with changes as high as 500%–1000% at  $V_{dc} < 1$  V. Interestingly, the shift of the ME peak to lower frequencies is accompanied by a significant reduction of its width near the critical voltage  $V^*$  inducing the magnetization reorientation. This feature is illustrated by Fig. 9 which shows the full width at half maximum (FWHM) of the peak of  $\text{Im}[\alpha_{33}(\nu)]$  plotted as a function of the applied voltage  $V_{dc}$ . Moreover, the electrical tuning of the resonance frequency becomes much more efficient near the voltage-induced SRT. Indeed, Fig. 10 shows that the tunability  $|\partial \nu_{res} / \partial E_3|$  of this frequency increases drastically at voltages  $V_{dc}$  close to the critical voltage  $V^*$ , reaching about 100 GHz/(V/nm) at  $V_{dc} = V^*$ . Therefore, ferromagnetic nanostructures with the voltage-controlled magnetic anisotropy are promising for the development of electrically tunable signal processing

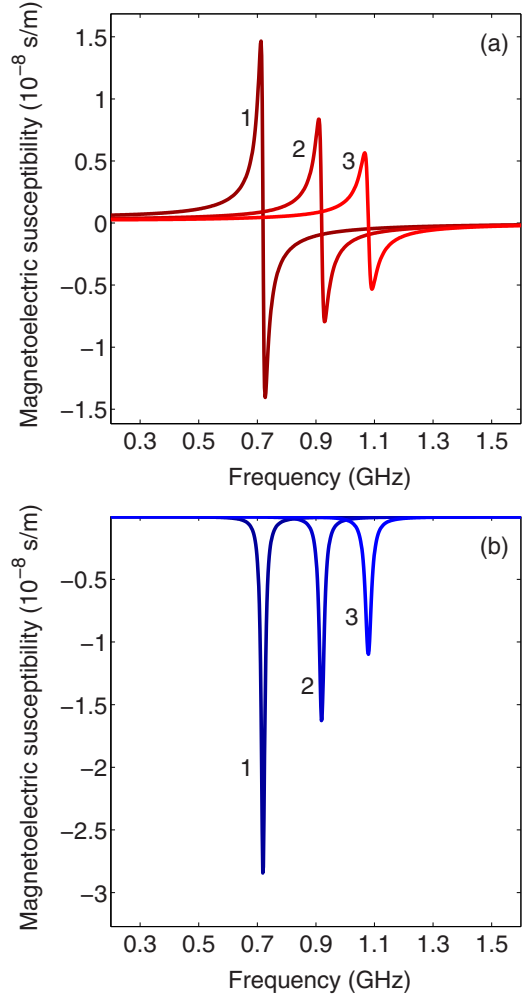


FIG. 6. (Color online) Evolution of the ME coefficient  $\alpha_{33}$  with the CoFeB layer thickness near the size-induced SRT. The real (a) and imaginary (b) parts of  $\alpha_{33}$  are plotted as functions of the frequency  $\nu$  of the driving ac voltage. The thickness of the CoFeB layer subjected to the magnetic field  $H_3 = 100$  Oe increases from  $t_f^* = 1.624$  nm (curve 1) to  $t_f = 1.674$  nm (curve 3) with the step  $\delta t_f = 0.025$  nm.

microwave devices with high tuning speed and low energy consumption, such as bandpass filters, phase shifters, resonant circuits in tunable oscillators, mixers, and frequency multipliers.

In the case of MTJs, the current created by the applied voltage is spin polarized so that an STT acts on the magnetization in addition to the torque caused by the effective field  $\mathbf{H}_{eff}$ . Therefore, the Landau-Lifshitz-Gilbert-Slonczewski equation should generally be used to describe the voltage-driven magnetization dynamics [17]. However, the analysis shows that the STT becomes comparable to the torque resulting from  $\Delta \mathbf{H}_{eff}(V)$  only in junctions with sufficiently high electrical conductances. Indeed, the STT factor  $\tau_{STT}$  (see Ref. [19]) for elastic tunneling in symmetric MTJs in the approximation of constant torque [3] can be written as  $\tau_{STT} = \gamma(\hbar/2e)[P/(1+P^2)]G_P V/t_f$ , where  $e$  is the electron charge,  $\hbar$  is the Planck constant,  $P$  is the spin polarization, and  $G_P$  is the MTJ conductance per unit area in the parallel state. Accordingly, the ratio  $\mathfrak{R} = \tau_{STT}/(\gamma\mu_0 M_s \Delta H_3^{eff}/m_3)$

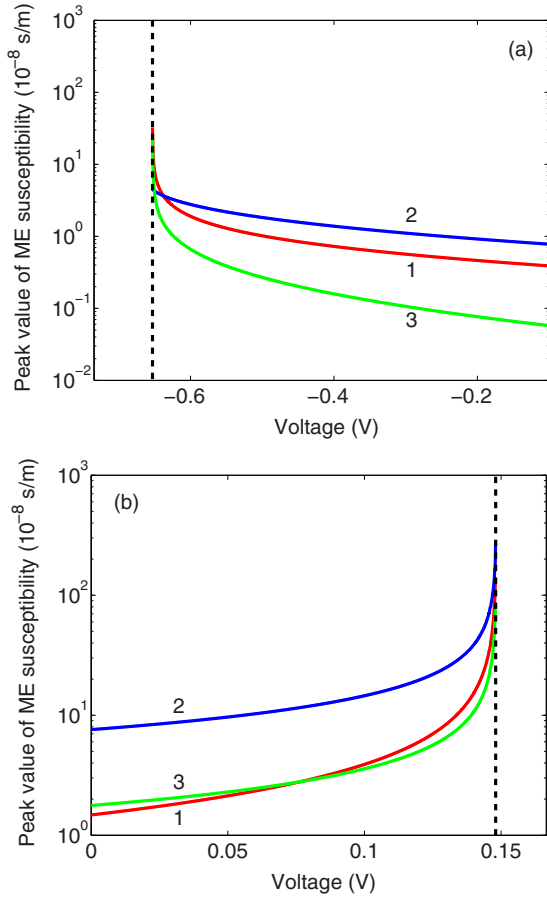


FIG. 7. (Color online) Peak values of the ME susceptibilities  $\text{Re}[\alpha_{i3}(v)]$  plotted as a function of the dc voltage applied to the CoFeB-MgO heterostructure. Panel (a) corresponds to the CoFeB layer with the thickness  $t_f = 1.545 \text{ nm} < t_f^*$  subjected to the magnetic field  $H_1 = 100 \text{ Oe}$ , whereas panel (b) shows the results obtained for the CoFeB thickness  $t_f = 1.73 \text{ nm} > t_f^*$  at the field  $H_3 = 700 \text{ Oe}$ . Curves 1, 2, and 3 show  $\text{Re}[\alpha_{13}(v_{\text{res}})]$ ,  $\text{Re}[\alpha_{23}(v_{\text{res}})]$ , and  $\text{Re}[\alpha_{33}(v_{\text{res}})]$ , respectively. The dashed line indicates the critical dc voltage  $V^*(t_f)$  inducing SRT.

characterizing the relative importance of two discussed torques may be estimated as  $\mathfrak{R} = -(\hbar/4e)[P/(1+P^2)](t_b/k_s)G_P$ . Using the parameters  $k_s = -50 \mu\text{J m}^{-2} (\text{V nm}^{-1})^{-1}$ ,  $t_b = 1 \text{ nm}$ , and  $P = 1/\sqrt{3}$  typical of CoFeB-MgO junctions, we find that  $\mathfrak{R}$  equals unity at a high conductance  $G_P \approx 5 \times 10^{11} \Omega^{-1} \text{ m}^{-2}$ . Therefore, there is a wide range of conductances, where the influence of STT on the voltage-driven magnetization dynamics can generally be neglected. This conclusion applies, for example, to the  $\text{Fe}_{80}\text{Co}_{20}/\text{MgO}$  junctions with  $G_P \sim 10^8 \Omega^{-1} \text{ m}^{-2}$  studied by Nozaki *et al.* [16]. On the other hand, the  $\text{Co}_{20}\text{Fe}_{60}\text{B}_{20}/\text{MgO}/\text{Co}_{40}\text{Fe}_{40}\text{B}_{20}$  junctions with  $G_P = 3 \times 10^{11} \Omega^{-1} \text{ m}^{-2}$ ,  $t_b = 0.83 \text{ nm}$ ,  $P = 0.54$  (Ref. [17]), and  $k_s = -33 \mu\text{J m}^{-2} (\text{V nm}^{-1})^{-1}$  (Ref. [15]) have  $\mathfrak{R} \approx 0.52$  so that the STT effect cannot be ignored, which agrees with the conclusion made in Ref. [17].

Importantly, MTJs with low conductances providing  $\mathfrak{R} \ll 1$  allow determining ME coefficients experimentally. This feature results from the phenomenon of magnetoresistance converting magnetization oscillations into an output dc voltage

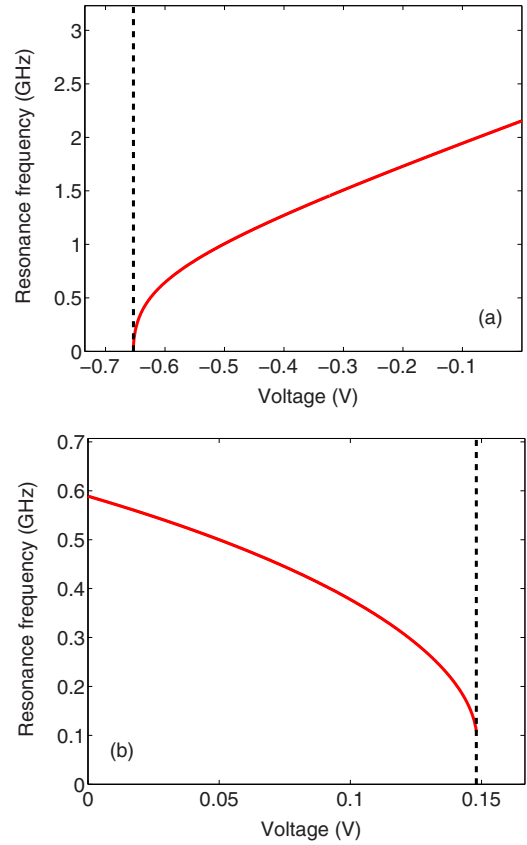


FIG. 8. (Color online) Resonance frequency of the magnetization precession as a function of dc voltage applied to the CoFeB-MgO heterostructure. The thickness of the CoFeB nanolayer equals  $1.579 \text{ nm} (t_f < t_f^*)$  (a) and  $1.629 \text{ nm} (t_f > t_f^*)$  (b). The applied magnetic field is  $H_1 = 100 \text{ Oe}$  (a) and  $H_3 = 700 \text{ Oe}$  (b). The dashed line here and below indicates the critical dc voltage  $V^*(t_f)$  inducing SRT.

$V_{\text{out}}$  measured by the homodyne detection technique [16]. In asymmetric MTJs, the conductance varies with the angle  $\psi$  between the magnetizations of two electrodes having the effective spin polarizations  $P_1$  and  $P_2$  as  $G = G_0(1 + P_1 P_2 \cos \psi)$  [2]. Using this formula together with Eqs. (7)–(9), we derived relations between  $\text{Re}[\alpha_{i3}]$  and  $V_{\text{out}}$ . For an MTJ with the PP fixed magnetization  $\mathbf{M}_{\text{fixed}} (\psi = \theta)$ , the calculation yields

$$\text{Re}[\alpha_{33}] \cong -\frac{2\mu_0 M_s t_b (1 + P_1 P_2 \cos \theta_0)}{P_1 P_2 \delta V_{\text{max}}^2} V_{\text{out}}. \quad (11)$$

If the applied magnetic field ensures the orientation of the free layer magnetization  $\mathbf{M}$  in the  $(x_1, x_3)$  plane ( $\phi_0 = 0$ ), the formula  $\text{Re}[\alpha_{13}] = -\cot \theta_0 \text{Re}[\alpha_{33}]$  renders it possible to evaluate  $\text{Re}[\alpha_{13}]$  via Eq. (11) as well. Alternatively, it can be found as

$$\text{Re}[\alpha_{13}] \cong -\frac{2\mu_0 M_s t_b}{P_1 P_2 \delta V_{\text{max}}^2} V_{\text{out}} \quad (12)$$

from the output voltage of an MTJ with  $\mathbf{M}_{\text{fixed}}$  parallel to the  $x_1$  axis and  $\mathbf{M}$  orthogonal to the  $x_2$  one. Finally,  $\text{Re}[\alpha_{23}] \cong -2\mu_0 M_s t_b V_{\text{out}} / (P_1 P_2 \delta V_{\text{max}}^2)$ , where  $V_{\text{out}}$  should be generated by a junction with  $\mathbf{M}_{\text{fixed}}$  and  $\mathbf{M}$  parallel and orthogonal to the  $x_2$  axis, respectively.

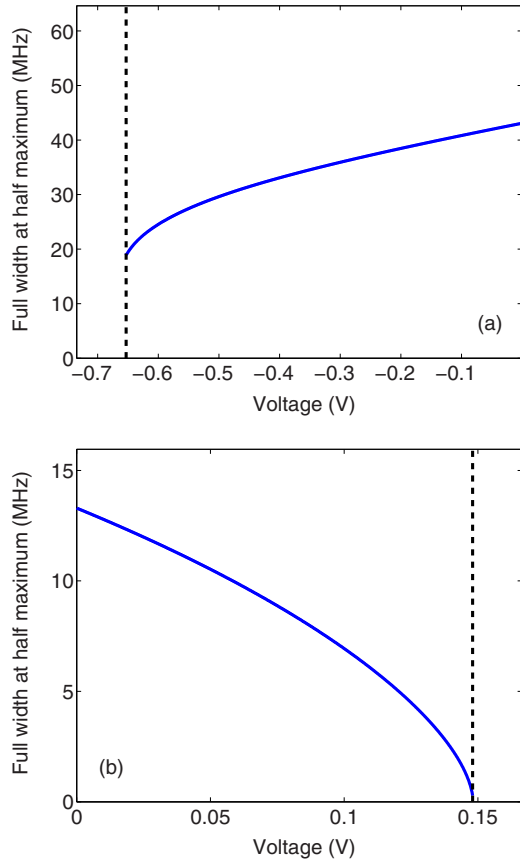


FIG. 9. (Color online) FWHM of the peak of  $\text{Im}[\alpha_{33}(v)]$  plotted as a function of dc voltage applied to the CoFeB-MgO heterostructure. The thickness of the CoFeB nanolayer equals 1.579 nm ( $t_f < t_f^*$ ) (a) and 1.629 nm ( $t_f > t_f^*$ ) (b). The applied magnetic field is  $H_1 = 100$  Oe (a) and  $H_3 = 700$  Oe (b).

#### IV. CONCLUDING REMARKS

In this paper, we described theoretically the ME effect in the form of voltage-induced magnetization oscillations in ferromagnetic nanostructures with electric-field-dependent interfacial anisotropy. Our calculations demonstrated that the real and imaginary parts of complex ME susceptibilities characterizing this effect display peaks at very close frequencies of the driving ac voltage. These characteristic frequencies may reduce dramatically near thickness-induced SRTs in ferromagnetic nanolayers, which is accompanied by a strong increase in the heights of ME peaks and their sharpness. Remarkably, the tunability of resonance frequency by dc voltages rises drastically near the critical voltage inducing an SRT. It should be emphasized that the precise control of nanolayer thickness ensuring  $t_f \cong t_f^*$  is not necessary for the observation of giant ME susceptibilities since the proximity to the SRT can be enhanced at a given  $t_f$  by applying appropriate dc voltage to an insulating layer.

The practical importance of our theoretical results is ensured by potential applications of considered nanostructures in various electronic devices. In particular, the predicted giant ME susceptibilities indicate that the sensitivity of microwave signal detectors based on MTJs [17,18] can be increased dramatically by making the free layer thickness  $t_f$

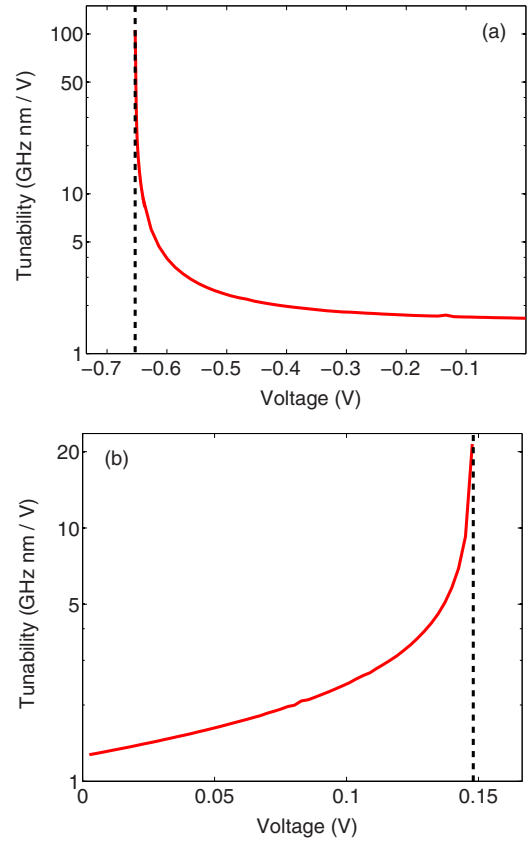


FIG. 10. (Color online) Tunability  $|\partial v_{\text{res}}/\partial E_3|$  of the resonance frequency as a function of dc voltage applied to the CoFeB-MgO heterostructure. The thickness  $t_f$  of the CoFeB nanolayer equals 1.545 nm ( $t_f < t_f^*$ ) (a) and 1.73 nm ( $t_f > t_f^*$ ) (b). The applied magnetic field is  $H_1 = 100$  Oe (a) and  $H_3 = 700$  Oe (b).

close to the critical thickness  $t_f^*$  or by applying a voltage approaching the critical voltage  $V^*(t_f)$ . For the detector sensitivity  $S_W$  given by the ratio of the output dc voltage  $V_{\text{out}}$  to the signal power  $W = GA\delta V_{\text{max}}^2$  ( $A$  is the electrode area), the calculation yields  $S_W = -P_1 P_2 \text{Re}[\alpha_{13}]/(\mu_0 M_s G A t_b)$  and  $S_W = -P_1 P_2 G_0 \text{Re}[\alpha_{33}]/(\mu_0 M_s G^2 A t_b)$  for MTJs with  $\mathbf{M}_{\text{fixed}}$  parallel to the  $x_1$  and  $x_3$  axis, respectively. Substituting here  $\text{Re}[\alpha_{i3}(v_{\text{res}})]$  given in Fig. 4, we find that, for CoFeB/MgO/CoFeB junctions similar to those studied in Ref. [17], the sensitivity  $S_W(v_{\text{res}})$  may exceed  $10^4$  V/W, which is about 20 times higher than the measured value reported in Ref. [17].

Furthermore, we propose a magnetic field sensor which utilizes the described dynamic converse ME effect in combination with the magnetoresistance of MTJs. Since the resonance frequency of the voltage-driven magnetization precession is highly sensitive to the external magnetic field  $\mathbf{H}$ , the output dc voltage  $V_{\text{out}}$  generated by the junction subjected to a microwave voltage  $V_{\text{ac}}$  of a fixed frequency  $\nu$  should vary with the field intensity  $H$ . Taking into account that  $V_{\text{out}}$  is directly proportional to  $\text{Re}[\alpha_{i3}]$ , we predict that the sensitivity  $\partial V_{\text{out}}/\partial H \sim (\partial \text{Re}[\alpha_{i3}]/\partial \nu)(\partial \nu/\partial H)$  will increase drastically near the frequency  $\nu_0$ . This feature demonstrates that CoFeB/MgO/CoFeB junctions can be employed as ultra-sensitive sensors of weak magnetic fields.

## ACKNOWLEDGMENTS

The work at the Ioffe Physical-Technical Institute was supported by the Government of the Russian Federation through the program P220 (project 14.B25.31.0025; leading scientist A. K. Tagantsev) and by the Russian Foundation for Basic Research (Grant No. 13-02-12429).

## APPENDIX A

The numerical calculations of voltage-induced magnetization oscillations were performed for (001)-oriented single-crystalline layers of cubic ferromagnets. The derivatives of the normalized free energy density  $f = F/(\mu_0 M_s^2)$  involved in Eqs. (3) and (4) were calculated via the formula [21]

$$\begin{aligned}
 F = & F_0 + K_1 m_1^2 m_2^2 + \left( K_1 + \frac{B_1^2}{2c_{11}} - \frac{B_2^2}{2c_{44}} \right) (m_1^2 + m_2^2) m_3^2 + K_2 m_1^2 m_2^2 m_3^2 + \frac{K_s}{t_f} m_3^2 \\
 & + B_1 (u_1 m_1^2 + u_2 m_2^2) + B_2 u_6 m_1 m_2 - B_1 \left[ \frac{B_1}{6c_{11}} + \frac{c_{12}}{c_{11}} (u_1 + u_2) \right] m_3^2 \\
 & + \frac{1}{2} \mu_0 M_s^2 (N_{11} m_1^2 + N_{22} m_2^2 + N_{33} m_3^2 + 2N_{12} m_1 m_2 + 2N_{13} m_1 m_3 + 2N_{23} m_2 m_3) \\
 & - \mu_0 M_s (H_1 m_1 + H_2 m_2 + H_3 m_3),
 \end{aligned} \tag{A1}$$

where  $F_0$  is the part of the energy density independent of the magnetization orientation, and  $m_1 = \cos\phi \sin\theta$ ,  $m_2 = \sin\phi \sin\theta$ ,  $m_3 = \cos\theta$  are the direction cosines of the magnetization  $\mathbf{M}$  with respect to the principal cubic axes  $x_i$  shown in Fig. 1 (note that  $m_1^2 + m_2^2 + m_3^2 = 1$ ). In Eq. (A1),  $N_{ik}$  are the components of the tensor of demagnetizing factors [25],  $K_1$  and  $K_2$  are the bulk magnetocrystalline anisotropy constants of fourth and sixth order at constant strains  $\mathbf{u}$  [26],  $K_s = K_{s0} + k_s V/t_b$  is the surface anisotropy parameter,  $B_1$  and  $B_2$  are the magnetoelastic coefficients, and  $c_{11}$ ,  $c_{12}$ , and  $c_{44}$  are the elastic stiffnesses at fixed  $\mathbf{M}$  (we use the Voigt matrix notation for strains and elastic constants). Since in this work the magnetization is taken to be uniformly distributed within the ferromagnetic nanolayer, the gradient energy  $A_{\text{ex}}[(\nabla m_1)^2 + (\nabla m_2)^2 + (\nabla m_3)^2]$  caused by the exchange coupling [27,28] was omitted in Eq. (A1). This approximation does not allow the description of inhomogeneous magnetic states and excitations, such as domain structures and spin waves, but is valid for magnetic layers with nanoscale in-plane dimensions and thicknesses smaller than the exchange length  $\lambda_{\text{ex}}$  [27,28]. Since the thicknesses  $t_f$  assumed in theoretical calculations are below 2 nm, whereas the exchange length of CoFe alloys is about 4 nm [28], the condition  $t_f < \lambda_{\text{ex}}$  is satisfied in our case.

For the material parameters involved in Eq. (A1), we employed the following values typical of CoFeB alloys:  $K_1 = 1.3 \times 10^4 \text{ J m}^{-3}$ ,  $K_2 = 0$ ,  $B_1 = -29.4 \times 10^6 \text{ J m}^{-3}$ ,  $B_2 = -3 \times 10^6 \text{ J m}^{-3}$ ,  $c_{11} = 2.8 \times 10^{11} \text{ N m}^{-2}$ ,  $c_{12} = 1.4 \times 10^{11} \text{ N m}^{-2}$ , and  $c_{44} = 1 \times 10^{11} \text{ N m}^{-2}$  [21]. The lattice strains in a CoFeB layer were assumed to be absent ( $u_1 = u_2 = u_6 = 0$ ), and the demagnetizing factors were taken to be  $N_{11} = N_{22} = 0.008$ ,  $N_{33} = 0.984$ , and  $N_{12} = N_{13} = N_{23} = 0$ , which correspond to square ferromagnetic layers with the in-plane dimensions of about 400 nm at the considered thicknesses  $t_f \approx 1.6 \text{ nm}$  [29]. The MgO thickness  $t_b$  was set equal to 0.8 nm.

Besides the calculations of voltage-induced magnetization oscillations, Eq. (A1) was used to determine the critical thickness  $t_f^*(V = 0)$  of the CoFeB layer and the critical dc voltage  $V^*(t_f)$  inducing the SRT in the presence of nonzero magnetic field  $\mathbf{H}$ . To this end, the magnetization orientations

corresponding to relevant local minima of the energy  $F(\phi, \theta)$  were calculated numerically as a function of the thickness  $t_f$  at a given  $\mathbf{H}$ , and the value of  $t_f^*(\mathbf{H})$  was then found as the thickness at which these minima acquire the same energy. This threshold situation is illustrated by Fig. 11, where the dependence of the energy density on the magnetization orientation is shown by a distribution of colors over the unit sphere for a representative CoFeB layer not subjected to any magnetic field.

The results obtained for CoFeB layers subjected to perpendicular-to-plane magnetic fields ( $H_3 > 0$ ) are shown in Fig. 12. In this situation, one of the energy minima is associated with the perpendicular-to-plane magnetization ( $\theta = 0$ ), whereas the other corresponds to a nonzero orientation angle  $\theta(H_3)$  that gradually decreases with increasing field intensity, as shown in Fig. 12(a). This variation is accompanied by a monotonic increase of the critical thickness  $t_f^*(H_3)$  continuing until the SRT disappears at the field  $H_3^* = 770 \text{ Oe}$  [Fig. 12(b)].

To check the validity of Eq. (A1) in the case of ultrathin ferromagnetic films, we calculated the critical thickness

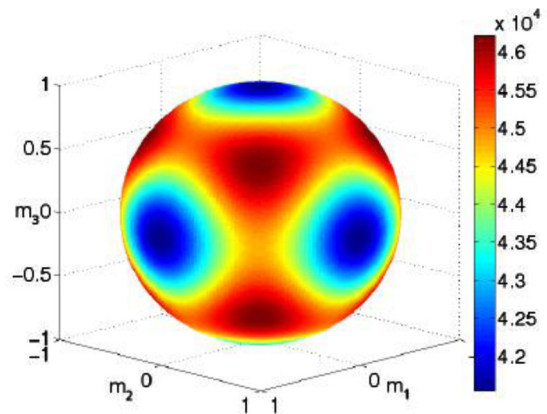


FIG. 11. (Color online) Dependence of the energy density on the magnetization orientation in a CoFeB layer with the critical thickness  $t_f^*(\mathbf{H} = 0) = 1.604 \text{ nm}$ .

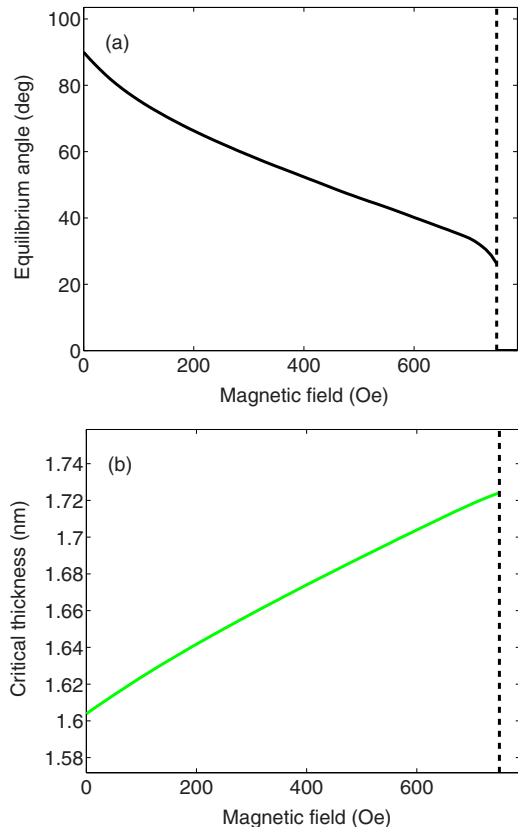


FIG. 12. (Color online) Effect of the applied magnetic field  $H_3$  on the orientation angle  $\theta$  characterizing inclined magnetization orientation in a CoFeB layer with the critical thickness  $t_f^*(H_3)$  (a) and the variation of  $t_f^*$  with the field intensity (b). The vertical dashed line indicates the critical field intensity  $H_3^* = 770$  Oe above which the SRT disappears.

$t_f^*(V = 0)$  for the  $\text{Co}_{20}\text{Fe}_{60}\text{B}_{20}/\text{MgO}$  heterostructures studied in Ref. [22]. With the measured magnetization  $M_s = 1.26 \times 10^6$  A m<sup>-1</sup> and the interfacial anisotropy  $K_{s0} = -1.3 \times 10^{-3}$  J m<sup>-2</sup> [22], the calculation gives  $t_f^* \approx 1.4$  nm, which is in good agreement with the measured value of about

1.5 nm [22]. The coercive field  $H_c(t_f)$  of the perpendicular-to-plane magnetization state, determined from the condition  $\partial^2 F / \partial \theta^2 = 0$ , was found to be in the order-of-magnitude agreement with the values  $H_c \sim 1$  kOe observed for the CoFeB/MgO/CoFeB junctions with the 40 nm diameter [22], where the magnetization switching is expected to develop through the coherent mode. These results support the validity of our approach.

## APPENDIX B

We also studied the magnetization oscillations induced by voltages periodically exceeding the critical voltage  $V^*(t_f)$ . Since at  $V = V^*$  the initial energy minimum transforms into a maximum, the magnetization will be destabilized even if its equilibrium direction at zero voltage is parallel or perpendicular to the surfaces of the ferromagnetic layer. Hence the magnetization will start to rotate towards another orientation corresponding to the adjacent energy minimum. This rotation, however, may be reversed by reducing the applied voltage back to a value well below  $V^*$  after a sufficiently short time. Indeed, the magnetization will be attracted to the initial energy minimum if the potential barrier between two energy minima reappearing during the voltage downswing was not crossed. Accordingly, a periodic voltage-driven motion of the magnetization can be excited.

Using an implicit Runge-Kutta method, we performed numerical simulations of the magnetization oscillations induced in the CoFeB-MgO heterostructure (at  $\mathbf{H} = 0$ ) by a sequence of unipolar voltage pulses with the magnitude  $V_{\text{max}} > V^*(t_f)$ . It was found that the voltage-driven oscillations have the form of an unsmooth rotation of the magnetization vector  $\mathbf{M}$  around the equilibrium direction. This feature is demonstrated by Fig. 13, where we plotted typical trajectory of the end of the unit vector  $\mathbf{m} = \mathbf{M}/M_s$  projected on the plane perpendicular to the equilibrium direction. Moreover, our simulations showed that a very precise control of the voltage time dependence is needed to induce steady magnetization oscillations of this sort. Therefore, it would be rather difficult to create such oscillations experimentally.

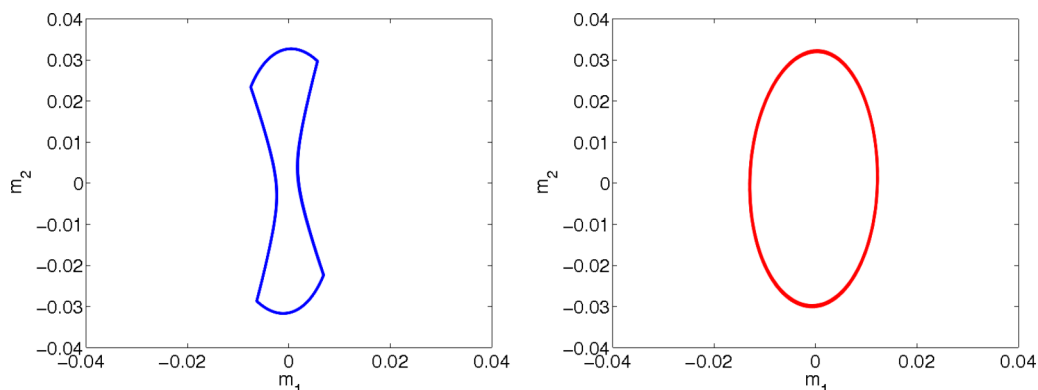


FIG. 13. (Color online) Typical trajectories of the end of the unit vector  $\mathbf{m} = \mathbf{M}/M_s$  projected on the plane perpendicular to an equilibrium direction of  $\mathbf{M}$ . The left panel corresponds to the unsmooth motion around the in-plane [100] direction induced by a sequence of unipolar voltage pulses with  $V_{\text{max}} > V^*(t_f)$ , whereas the right panel characterizes the magnetization precession around an inclined equilibrium direction driven by a weak ac voltage  $V_{\text{ac}} \ll V^*(t_f)$ .

- [1] M. Farle, *Rep. Prog. Phys.* **61**, 755 (1998).
- [2] J. C. Slonczewski, *Phys. Rev. B* **39**, 6995 (1989).
- [3] J. C. Slonczewski and J. Z. Sun, *J. Magn. Magn. Mater.* **310**, 169 (2007).
- [4] S. I. Kiselev, J. C. Sankey, I. N. Krivorotov, N. C. Emley, R. J. Schoelkopf, R. A. Buhrman, and D. C. Ralph, *Nature (London)* **425**, 380 (2003).
- [5] W. H. Rippard, M. R. Pufall, S. Kaka, S. E. Russek, and T. J. Silva, *Phys. Rev. Lett.* **92**, 027201 (2004).
- [6] M. Deac, A. Fukushima, H. Kubota, H. Maehara, Y. Suzuki, S. Yuasa, Y. Nagamine, K. Tsunekawa, D. D. Djayaprawira, and N. Watanabe, *Nat. Phys.* **4**, 803 (2008).
- [7] P. M. Braganca, O. J. Lee, O. Ozatay, L. Liu, G. Finocchio, D. C. Ralph, and R. A. Buhrman, *Appl. Phys. Lett.* **102**, 252402 (2013).
- [8] J. C. Sankey, P. M. Braganca, A. G. F. Garcia, I. N. Krivorotov, R. A. Buhrman, and D. C. Ralph, *Phys. Rev. Lett.* **96**, 227601 (2006).
- [9] J. C. Sankey, Y.-T. Cui, J. Z. Sun, J. C. Slonczewski, R. A. Buhrman, and D. C. Ralph, *Nat. Phys.* **4**, 67 (2008).
- [10] M. Weisheit, S. Fähler, A. Marty, Y. Souche, C. Poinsignon, and D. Givord, *Science* **315**, 349 (2007).
- [11] C.-G. Duan, J. P. Velev, R. F. Sabirianov, Z. Zhu, J. Chu, S. S. Jaswal, and E. Tsymbal, *Phys. Rev. Lett.* **101**, 137201 (2008).
- [12] T. Maruyama, Y. Shiota, T. Nozaki, K. Ohta, N. Toda, M. Mizuguchi, A. A. Tulapurkar, T. Shinjo, M. Shiraishi, S. Mizukami, Y. Ando, and Y. Suzuki, *Nat. Nanotechnol.* **4**, 158 (2009).
- [13] K. Nakamura, R. Shimabukuro, Y. Fujiwara, T. Akiyama, T. Ito, and A. J. Freeman, *Phys. Rev. Lett.* **102**, 187201 (2009).
- [14] M. K. Niranjan, C.-G. Duan, S. S. Jaswal, and E. Y. Tsymbal, *Appl. Phys. Lett.* **96**, 222504 (2010).
- [15] S. Kanai, M. Yamanouchi, S. Ikeda, Y. Nakatani, F. Matsukura, and H. Ohno, *Appl. Phys. Lett.* **101**, 122403 (2012).
- [16] T. Nozaki, Y. Shiota, S. Miwa, S. Murakami, F. Bonell, S. Ishibashi, H. Kubota, K. Yakushiji, T. Saruya, A. Fukushima, S. Yuasa, T. Shinjo and Y. Suzuki, *Nat. Phys.* **8**, 491 (2012).
- [17] J. Zhu, J. A. Katine, G. E. Rowlands, Y.-J. Chen, Z. Duan, J. G. Alzate, P. Upadhyaya, J. Langer, P. K. Amiri, K. L. Wang, and I. N. Krivorotov, *Phys. Rev. Lett.* **108**, 197203 (2012).
- [18] A. Tulapurkar, Y. Suzuki, A. Fukushima, H. Kubota, H. Maehara, K. Tsunekawa, D. D. Djayaprawira, N. Watanabe, and S. Yuasa, *Nature (London)* **438**, 339 (2005).
- [19] N. A. Pertsev, *Sci. Rep.* **3**, 2757 (2013).
- [20] M. D. Stiles and J. Miltat, in *Spin Dynamics in Confined Magnetic Structures III*, edited by B. Hillebrands and A. Thiaville, *Topics in Applied Physics* (Springer, Berlin, 2006), Vol. 101, pp. 225–308.
- [21] N. A. Pertsev and H. Kohlstedt, *Adv. Funct. Mater.* **22**, 4696 (2012).
- [22] S. Ikeda, K. Miura, H. Yamamoto, K. Mizunuma, H. D. Gan, M. Endo, S. Kanai, J. Hayakawa, F. Matsukura, and H. Ohno, *Nat. Mater.* **9**, 721 (2010).
- [23] W.-G. Wang, M. Li, S. Hageman, and C. L. Chien, *Nat. Mater.* **11**, 64 (2012).
- [24] N. A. Pertsev, H. Kohlstedt, and R. Knöchel, *Phys. Rev. B* **84**, 014423 (2011).
- [25] L. D. Landau, E. M. Lifshitz, and L. P. Pitaevskii, *Electrodynamics of Continuous Media* (Pergamon, Oxford, 1984).
- [26] N. A. Pertsev, *Phys. Rev. B* **78**, 212102 (2008).
- [27] B. Heinrich and J. F. Cochran, *Adv. Phys.* **42**, 523 (1993).
- [28] C. A. F. Vaz, J. A. C. Bland, and G. Lauthoff, *Rep. Prog. Phys.* **71**, 056501 (2008).
- [29] A. Aharoni, *J. Appl. Phys.* **83**, 3432 (1998).